

Statistical Analysis of Interference for Nanoscale Electromechanical Wireless Communication at VHF-Band

Janne J. Lehtomäki, *Member, IEEE*, A. Ozan Bicen, *Student Member, IEEE*, and Ian F. Akyildiz, *Fellow, IEEE*

Abstract—Nanoscale electromechanical wireless communication with on-off keying in the very high frequency (VHF) band (30–300 MHz) is studied for a receiver using a carbon nanotube (CNT). Previous studies on this topic have only considered continuous wave (CW) on-off keying which suffers from spectral widening due to sharp changes in the signal. Effects of the inter-symbol interference (ISI), the co-channel interference, and the adjacent channel interference on the received signal statistics have not been analyzed. The rise- and fall-times associated with the filtering of the incoming signal by the mechanical frequency response of the receiver's CNT have also been ignored. In this paper, Fourier-series based modeling and statistical analysis of decision variables are performed. The results and modeling in this study enable performance evaluation of CNT based receivers with an arbitrary number of interfering signals with arbitrary pulse shapes, and fully incorporates the transient signal components. Received signal statistics under interference are derived using the developed model. Numerical results are presented for Hanning pulse and trapezoidal pulse (which includes rectangular pulses corresponding to CW as a special case). The required guard intervals between pulses to mitigate ISI, required frequency separation between channels, and required spatial separation of co-channel networks (frequency reuse distance) are shown. These results show that large frequency reuse distance is required, limiting efficient spectrum utilization. However, the ISI and adjacent channel interference can be controlled more easily with a proper selection of parameters.

Index Terms—Carbon nanotube, frequency division multiple access, on-off keying, nanodevice, nanonetwork, VHF-band, wireless communication.

Manuscript received May 26, 2015; revised October 05, 2015; accepted December 10, 2015. Date of publication December 25, 2015; date of current version March 02, 2016. The associate editor coordinating the review of this manuscript and approving it for publication was Prof. Weifeng Su. The work of JL is supported by SeCoFu project of the Academy of Finland. The work of IFA and AOB is supported by the Academy of Finland FiDiPro (Finnish Distinguished Professor) program, for the project “Nanocommunication Networks,” 2012–2016.

J. Lehtomäki is with the Centre for Wireless Communications (CWC), Department of Communications Engineering, University of Oulu, Oulu 90014, Finland (e-mail: jannel@ee.oulu.fi).

A. O. Bicen and I. F. Akyildiz are with the Nano Communications Center, Department of Electronics and Communications Engineering (TUT-NCC), Tampere University of Technology, Tampere, FI-32720, Finland, and also with Broadband Wireless Networking Lab, School of Electrical and Computer Engineering, Georgia Institute of Technology, Atlanta, GA, 30332 USA (e-mail: bozan@ece.gatech.edu; ian@ece.gatech.edu).

Color versions of one or more of the figures in this paper are available online at <http://ieeexplore.ieee.org>.

Digital Object Identifier 10.1109/TSP.2015.2512526

I. INTRODUCTION

NANODEVICES consist of nanoscale components. Since the nanodevices are minuscule, they have very limited capabilities such as transistor count, e.g., a nanowire computer with 180 transistors has been demonstrated in [1]. Nanonetworks consisting of several nanodevices wirelessly communicating and cooperating with each other can collectively conduct more complex operations [2]–[5]. To this end, the use of carbon nanotube (CNT) radio to realize nanoscale communication is a promising paradigm as demonstrated in [6]–[9]. The most fundamental receiver components for electromagnetic communication in the very high frequency (VHF) (30–300 MHz) band (antenna, filter, amplifier, and demodulator) can all be implemented with a CNT. The first CNT based receiver was demonstrated in [6] for wireless audio signal reception with a CNT of approximately 500 nm long. Recently, nanopillars have been considered instead of the CNTs in [10] and the reception of audio signals was demonstrated.

The bit error probability (BEP) for the nanotube receiver with on-off keying was first investigated in [7], [8]. In [9], the communication theoretical analysis of nanotube receiver was extended to include both square-law and linear components present in the CNT based receivers and the exact noise correlation model was utilized. In these papers, bits 1 and 0 are transmitted by simply switching on or off a carrier depending on the current bit: this can also be called a interrupted continuous wave (CW) and BEP is evaluated without any interfering signals.

In this paper, statistical analysis of the CNT based digital communication is performed by providing a framework to determine the BEP under an arbitrary number of interfering signals. The statistical analysis is enabled by representing the decision variable based on integration of the time-domain signals and noise as a sum of quadratic (matrix) form, linear form, and the constant component, where the input to the matrix operations is the Fourier series representation of the input signals and thermomechanical noise. We find the Fourier series representation of the input signals and derive the covariance matrix of the Fourier series coefficients of the thermomechanical noise. The random carrier phases of the signals present are also represented as matrix operations, enabling the derivation of the statistics of the decision variable in the realistic case with random carrier phases. To the best of our knowledge, this is the first work on

CNT based reception focusing on statistical analysis under interference. Our main contributions are:

- 1) We use Fourier series-based modeling which allows extending the previous models for CNT based receivers by fully including transient effects, which are due to the filtering of the input pulses by the receiver's carbon nanotube, leading to rise- and fall-times in the output,
- 2) We consider inter-symbol interference (ISI), adjacent channel interference, and co-channel interference. Previously, no interference analysis has been performed. The Fourier-series based modeling enables us to model the received signal in the presence of multiple arbitrary interfering signals.

Based on the results, we noticed that the CNT based receiver experiences substantial performance degradation due to frequency reuse. On the other hand, the required frequency separation between channels was found to be reasonable, and required guard time between pulses to suppress ISI, which was also found to be rather small.

The remainder of this paper is organized as follows: In Section II, we present background on the Fourier series and on the properties of CNTs needed in the remainder of the paper. The output of an average-level detector under interference is found in Section III as a function of the Fourier series coefficients of the CNT tip vertical displacement $y(t)$. The theoretical mean and variance of the detector output are found in Section IV. Based on the Gaussian approximation, the BEP in the presence of an arbitrary number of interfering pulses is derived in Section V. Numerical results are shown in Section VI presenting BEP under ISI, adjacent channel interference, and co-channel interference. Finally, conclusions are drawn in Section VII.

II. BACKGROUND

We consider a transmitter capable of sending electromagnetic (EM) radiation. To indicate bit 1, the transmitter transmits a waveform of duration T and no transmission corresponds to bit 0. The relation of nanoscale on-off keying to impulse radio is described in Section II.A. The basics of Fourier series needed for the rest of paper are discussed in Section II.B. The utilized baseband pulse shapes to indicate bit 1 are discussed in Section II.C. The relationship between the electric field strength (due to the EM radiation) and the mechanical oscillation is given by the mechanical transfer function in Section II.D, where the Fourier series based approach is used. The mechanical oscillation of the CNT leads to time-varying output signal which can be used to detect the transmitted bit (1 or 0). The details of CNT based reception are given in our previous paper [9].

A. Relation to Impulse Radio

An ultrawideband (UWB) impulse radio (IR) with on-off keying and energy detection has been studied [11]. The generic problems related to threshold setting and selection of integration window have been considered in [12]. In carrier-based IR-UWB, the output waveform is generated by modulating a local oscillator with, e.g., rectangular and triangular pulse

shapes [13]. The rectangular pulse shape requires extra filtering to achieve sufficient sidelobe rejection [13]. There are many significant differences to carrier-based IR-UWB meriting new analysis. For example,

- 1) In IR-UWB, the main effect to consider for ISI is the multipath channel and its delay spread. Transient response is less important. In the case of nanoscale VHF-Band reception, the situation is the opposite. For example, for the parameters we consider, the pulse duration is around 7000 ns and transient response is around 3000 ns. Typical maximum multipath delay, for example, for body area networks is less than 100 ns [12]. This means a signal spends more time inside the receiver circuit than in wireless propagation.
- 2) Typically, IR-UWB models assume additive white Gaussian noise [11]. This is not a valid assumption for nanoscale VHF-Band reception as the thermomechanical noise is strongly non-white.
- 3) The energy detection receiver for IR-UWB does not consider linear components [11]. In nanoscale VHF-Band reception, both square-law and linear components are present.

B. Fourier Series

Since it is used in the remainder of this paper, we show here the standard Fourier series representation of an arbitrary time-varying function $y(t)$ in the interval $t \in [0, T_P]$

$$y(t) = \frac{a_0}{2} + \sum_{n=1}^N \left[a_n \cos\left(\frac{2\pi nt}{T_P}\right) + b_n \sin\left(\frac{2\pi nt}{T_P}\right) \right], \quad (1)$$

where N/T_P is the highest frequency and real-valued Fourier series coefficients a_n and b_n are obtained with the standard approach [14]. It is emphasized that t outside the studied interval $[0, T_P]$ does not matter: the analysis we performed in the studied interval is assumed to be sufficient. Let us collect all the Fourier series coefficients in a column vector with $2N + 1$ elements

$$\vec{x} = [a_0 \ a_1 \ \dots \ a_N \ b_1 \ \dots \ b_N]^T, \quad (2)$$

where $(\cdot)^T$ represents matrix transpose and we use $\vec{\cdot}$ to indicate real-valued Fourier series coefficients.

The complex-valued Fourier coefficients c_n are [14]

$$c_n = \frac{1}{T_P} \int_0^{T_P} y(t) \cdot \exp\left(\frac{-i2\pi nt}{T_P}\right) dt, \quad (3)$$

where $i = \sqrt{-1}$. Let us collect them in a $N + 1$ vector

$$\hat{\vec{x}} = [c_0 \ c_1 \ \dots \ c_N]^T. \quad (4)$$

In the remainder of this paper, $\hat{\cdot}$ always denotes complex-valued Fourier series. The real-valued coefficients are obtained from complex-valued ones with

$$a_0 = 2c_0, \ a_n = 2\text{Re}(c_n), \ b_n = -2\text{Im}(c_n).$$

Let us denote the operator mapping $N + 1$ complex valued coefficients to $2N + 1$ real-valued ones with Γ , e.g., $\vec{x} = \Gamma(\hat{\vec{x}})$.

C. Baseband Pulse Shapes Modulated by a Carrier Frequency Cosine

Fourier series can be found for arbitrary pulse shapes. However, without loss of generality, we focus on transmitted signals generated by modulating a carrier frequency cosine with a pulse shape, i.e.,

$$s(t) = \cos(2\pi f_c t + \theta)p(t), \quad 0 \leq t \leq T, \quad (5)$$

where θ is the carrier phase, T is the pulse duration, f_c is the carrier frequency, and $p(t)$ is the basic baseband pulse shape (e.g., rectangular pulse). Since on-off keying is considered, the transmission of the signal $s(t)$ corresponds to bit 1 and no transmission during $0 \leq t \leq T$ corresponds to bit 0. There can be additional guard time δ between adjacent bits to reduce ISI, so the total pulse separation is $T + \delta$. By plugging in the transmitted signal to (3) and by using the modulation theorem of Fourier transform we obtain

$$c_n = \frac{1}{2T_P} \left(F_{\text{PULSE}} \left(\frac{n}{T_P} - f_c \right) + F_{\text{PULSE}} \left(\frac{n}{T_P} + f_c \right) \right), \quad (6)$$

where F_{PULSE} is the Fourier transform of $p(t)$ and the Fourier series index n corresponds to frequency n/T_P .

D. Mechanically Filtered Pulse Shapes at the Receiver

By using the theory of damped harmonic oscillators as in [15], the transfer function of the CNT's mechanical response to the incoming signal (electric field) is found to be

$$H_{\text{mech}}(s) = \frac{q/m_{\text{eff}}}{s^2 + \frac{\omega_0}{Q}s + \omega_0^2}, \quad (7)$$

where m_{eff} is the effective mass of the CNT, and ω_0 is the mechanical resonance frequency of the CNT (in radians), Q is the quality factor of the CNT, and q the charge at the tip of the CNT.

The complex Fourier series coefficients of the output of a linear time-invariant (LTI) system are obtained by multiplying the input Fourier series coefficients with the frequency response of the LTI. Thus, the complex Fourier series coefficients of the filtered signal are

$$c_n^{\text{out}} = H_{\text{mech}} \left(i \frac{2\pi n}{T_P} \right) \cdot c_n, \quad (8)$$

where c_n are the Fourier series coefficients of the input given in (6). Let us denote the vector containing the complex-valued coefficients c_n^{out} , $n = 0, \dots, N$ as $\hat{\mathbf{s}}$, i.e.,

$$\hat{\mathbf{s}} = [c_0^{\text{out}} \ c_1^{\text{out}} \ \dots \ c_N^{\text{out}}]^T \quad (9)$$

and let us denote the corresponding real-valued coefficient vector as

$$\vec{\mathbf{s}} = \Gamma(\hat{\mathbf{s}}). \quad (10)$$

By using these coefficients, the Fourier series can be evaluated at arbitrary points in time with (1) to get the time-variant output after the CNT in the interval $t \in [0, T_P]$.

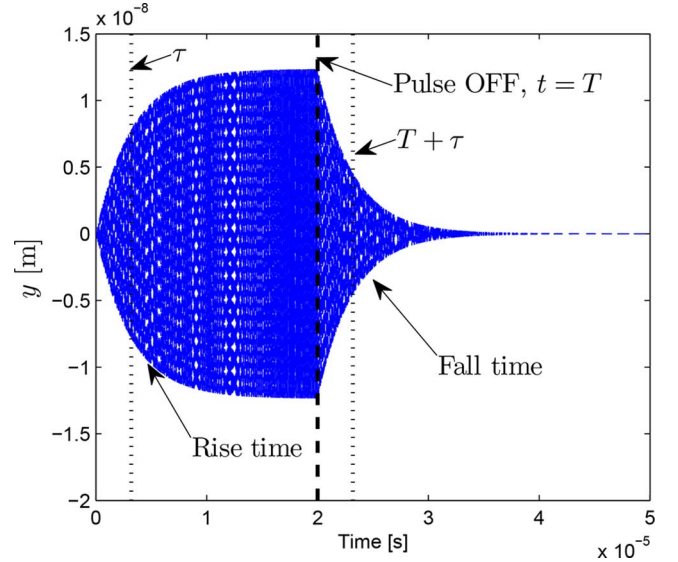


Fig. 1. Vertical CNT tip displacement $y(t)$ for rectangular input pulse. Carrier frequency $f_c = 20$ MHz. Pulse duration $T = 2 \times 10^{-5}$ [s], Fourier series period $T_P = 5 \times 10^{-5}$ [s]. CNT quality factor $Q = 200$ and resonance frequency in radians $\omega_0 = 2\pi \cdot 20 \times 10^6$ (20 MHz).

Fig. 1 shows a CW signal (carrier frequency cosine modulated by rectangular pulse shape) after filtering by the CNT. The vertical axis corresponds to the vertical displacement of the CNT tip as a function of time. The time constant of the CNT filter, i.e., time required for the output to rise to 63% of its steady-state output (or fall to 37%) for rectangular pulse, is $\tau = 2Q/\omega_0$ [15].

The Fourier series period T_P needs to be sufficiently larger than the duration T of the pulse shape used for on-off keying, so that transient components are included, e.g., in Fig. 1 for $T = 2 \times 10^{-5}$, $T_P = 5 \times 10^{-5}$ is used.

E. Thermomechanical Noise at the Receiver

The thermomechanical noise causes the CNT tip to oscillate even without input electric field. Let us denote the vertical displacement of the CNT tip due to thermal energy by $y_{\text{noise}}(t)$, modeled as non-white Gaussian process. Based on the equipartition theorem [15]

$$\mathbb{E} [y_{\text{noise}}(t)^2] = \frac{k_B T_K}{m_{\text{eff}} \omega_0^2}, \quad (11)$$

where $\mathbb{E}[\cdot]$ denotes expectation, k_B is the Boltzmann constant, and T_K is the temperature in Kelvin. It is shown in [9] that the autocorrelation of $y_{\text{noise}}(t)$ is

$$C_{y_{\text{noise}}}(x) = \mathbb{E}[y_{\text{noise}}(t)^2] \cdot \left(\frac{ue^{-|x|v} - ve^{-|x|u}}{u - v} \right), \quad (12)$$

where

$$u = \frac{\omega_0}{2Q} - i \frac{\omega_0 (\sqrt{4Q^2 - 1})}{2Q}, \quad v = u^*, \quad (13)$$

where $(\cdot)^*$ denotes complex conjugate and $Q > 1/2$.

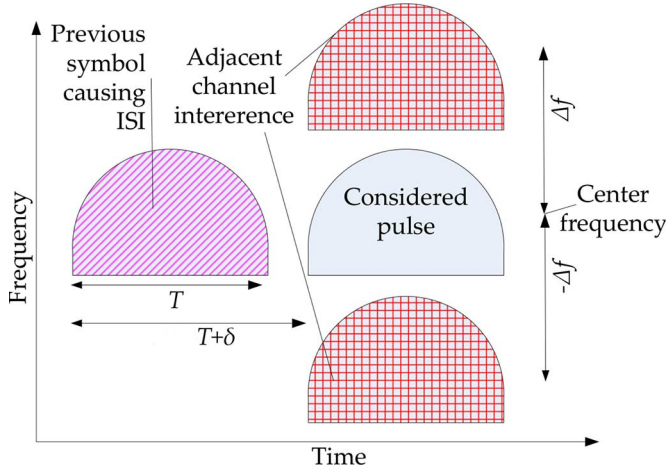


Fig. 2. Two adjacent channel interfering signals and intersymbol interference from previous pulse, $M_T = 4$. Bit duration $T + \delta$, where T is pulse duration and δ is extra pulse separation to reduce intersymbol interference. Frequency channel separation Δf , where typically $\Delta f > 1/T$ to reduce adjacent channel interference.

III. DECISION STATISTIC UNDER INTERFERENCE

A. Interfering Signals

We assume $M_T - 1$ interfering signal sources (which can be on or off depending on their current bit, so the number of current active signals M varies from 0 to M_T). We consider adjacent channel interference, co-channel interference, and ISI. The adjacent channel interference refers to the interference due to spectral leakage from on-going transmissions in adjacent frequency channels (above or below the studied channel). The co-channel interference refers to interference from on-going transmissions in the same frequency channel but with some spatial separation (distance) to the studied receiver. The ISI refers to interference from our own previous pulse, due to its tail response overlapping with the current pulse.

Fig. 2 illustrates two adjacent channel interfering signals (above and below the considered channel) and our previous pulse (source of ISI). We emphasize that in the case shown in the Fig. 2, the instantaneous number of signal components M varies from 0 to 4. When our current and previous bits are 0 (off, silence) and also both interfering transmitters currently have bit 0, then no signal components are present (only silence). When all the bits are 1, then there are 4 signal components and this is the case illustrated in Fig. 2.

B. Signal Model

Let us denote the time-varying CNT-tip vertical displacement as $y(t)$, which is assumed to consist of the thermomechanical noise and M signals ($M = 0$ refers to noise-only case), i.e.,

$$y(t) = \sum_{i=1}^M h_{\text{mech}}(t) * (E_{\text{rad},i} s_i(t)) + y_{\text{noise}}(t), \quad (14)$$

where $h_{\text{mech}}(t)$ is the impulse response of the CNT, $*$ denotes convolution, $E_{\text{rad},i}$ is the scaling factor to get the distance and transmit power dependent received electric field strength as given in ([9], (17)), and $s_i(t)$ are the signals following (5).

The carrier phases θ_i of the signals are assumed to be independent and identically distributed uniform random variables in the interval $[0, 2\pi]$. The signals can have different time and frequency offsets, enabling the study of interference effects. When ISI is evaluated, T_P needs to be sufficient to include also the previous pulse duration and a guard interval δ between pulses. When interference is evaluated from adjacent higher frequency channel, the number of Fourier series terms needs to be increased to achieve sufficient oversampling.

The Fourier series coefficients of $y(t)$ in the considered interval $t \in [0, T_P]$ are

$$\vec{x} = \vec{m} + \vec{n}, \quad (15)$$

where

$$\vec{m} = \sum_{i=1}^M E_{\text{rad},i} \vec{s}_i, \quad (16)$$

where \vec{s}_i are obtained with (10) and do include multiplication by the mechanical frequency response $H_{\text{mech}}(i \frac{2\pi n}{T_P})$ in (8) to represent the time domain convolution, so the transient effects are included. See, for example, Fig. 1. A possible time offset t_s is represented by multiplying the complex-valued Fourier coefficients with $\exp(-i \frac{2\pi n t_s}{T_P})$, leading to replacing (8) with

$$c_n^{\text{out}} = H_{\text{mech}} \left(i \frac{2\pi n}{T_P} \right) \exp \left(-i \frac{2\pi n t_s}{T_P} \right) \cdot c_n, \quad (17)$$

The coefficients c_n represent arbitrary signals. For example, for baseband pulse shapes modulated by a carrier frequency cosine, the coefficients are given in (6), where F_{PULSE} is the Fourier transform of an arbitrary baseband pulse shape $p(t)$ and f_c is an arbitrary carrier frequency of the signal. In case of adjacent channel interference, the carrier frequency of the interfering signals is different from the carrier frequency of the desired signal, i.e., the carrier frequency used in (6) differs from the f_c of the studied signal. We assume that the carrier phase rotation is represented by multiplication of complex Fourier series coefficients of the signal i with $\exp(i\theta_i)$. The vector \vec{n} contains the real-valued Fourier coefficients of the thermomechanical noise. As the thermal displacement noise is modeled as non-white Gaussian, the Fourier coefficients follow the zero-mean multivariate Gaussian distribution, i.e., $\vec{n} \sim \mathcal{N}(\mathbf{0}, \Sigma)$, where the covariance matrix Σ is derived in the Appendix A.

C. Output Current and Decision Statistic

The output current of the CNT based receiver, due to the field emission effect, is affected by the $y(t)$. The output current can be accurately approximated with [9], [16].

$$I(y(t)) = I_0 \alpha_2 y(t)^2 + I_0 \alpha_1 y(t) + I_0, \quad (18)$$

where α_1 and α_2 are presented in [9]. Similar to [7], we use an average-level detector at the receiver for detecting the on-off keyed digital communication signal. The utilized decision statistic is

$$\xi(y(t)) = \frac{1}{T_{\text{int}}} \int_{t=\epsilon}^{T_{\text{int}}+\epsilon} I(y(t)) dt, \quad (19)$$

where T_{int} is the integration duration and ϵ is the starting time for integration. The integration window is the time interval $[\epsilon T_{\text{int}} + \epsilon]$. It is important to note that the optimal window is not necessarily equal to $[0 T]$ (where T is the pulse duration) since, for example, the transient components affect it shifting the optimal integration window to the right. See, for example, Fig. 1.

In Appendix B, we derive a matrix theoretical representation of the decision statistic. The result is

$$\xi(\vec{x}) = \vec{x}^T \mathbf{A} \vec{x} + \mathbf{b} \vec{x} + I_0, \quad (20)$$

where \vec{x} is given in (15). The decision statistic ξ is given in integral form in (19) and equivalently in matrix form in (20).

IV. MEAN AND VARIANCE OF THE DECISION STATISTIC

The signal model (14) consists of thermomechanical noise and M signals. We derive both the theoretical mean $\mathbb{E}[\xi]$ in (28) and theoretical variance $\text{Var}[\xi]$ in (32) (by using (45)), both in the presence of M of signals, where $M \geq 0$ is an arbitrary integer. Our derivations take into account random and independent carrier phases of the signals, making the analysis more challenging. The mean and variance will be used in Section V to obtain the bit error probability through the Gaussian approximation.

A. Conditional Mean and Variance

Let us first derive the conditional mean and variance assuming that $\vec{\mathbf{m}}$ in (16) is fixed, so that only randomness in the decision statistic (20) is due to the thermomechanical noise present in \vec{x} , i.e., $\vec{\mathbf{n}}$. By standard matrix theory for the mean of quadratic and linear forms [17],

$$\mathbb{E}[\xi | \vec{\mathbf{m}}] = \mu_{\text{noise}} + \vec{\mathbf{m}}^T \mathbf{A} \vec{\mathbf{m}} + \mathbf{b} \vec{\mathbf{m}}, \quad (21)$$

where the noise-only component

$$\mu_{\text{noise}} = \text{Tr}(\mathbf{A} \Sigma) + I_0 \quad (22)$$

and Tr denotes matrix trace. Closed form expression for μ_{noise} has been presented in ([9], (30)).

The constant component I_0 can be ignored when finding variance. By standard results for the variance of a sum of two correlated random variables,

$$\begin{aligned} \text{Var}[\xi | \vec{\mathbf{m}}] &= \text{Var}[\vec{x}^T \mathbf{A} \vec{x}] + \text{Var}[\mathbf{b} \vec{x}] \\ &\quad + 2\mathbb{E}[\vec{x}^T \mathbf{A} \vec{x} \cdot \mathbf{b} \vec{x}] \\ &\quad - 2\mathbb{E}[\vec{x}^T \mathbf{A} \vec{x}] \mathbb{E}[\mathbf{b} \vec{x}] \\ &= \text{Var}_{\text{noise}} + 2\mathbf{b} \Sigma (\mathbf{A} + \mathbf{A}^T) \vec{\mathbf{m}} \\ &\quad + \vec{\mathbf{m}}^T (\mathbf{A} + \mathbf{A}^T) \Sigma (\mathbf{A} + \mathbf{A}^T) \vec{\mathbf{m}}, \end{aligned} \quad (23)$$

where

$$\text{Var}_{\text{noise}} = \text{Tr}(\mathbf{A} \Sigma (\mathbf{A} + \mathbf{A}^T) \Sigma) + \mathbf{b} \Sigma \mathbf{b}^T. \quad (24)$$

Closed form expression for $\text{Var}_{\text{noise}}$ is in ([9], (33)). In the derivation above, we use the properties of a multivariate Gaussian with mean vector $\vec{\mathbf{m}}$ [17] leading to

$$\mathbb{E}[\vec{x}^T \mathbf{A} \vec{x}] \mathbb{E}[\mathbf{b} \vec{x}] = \text{Tr}(\mathbf{A} \Sigma) \cdot \mathbf{b} \vec{\mathbf{m}} + \vec{\mathbf{m}}^T \mathbf{A} \vec{\mathbf{m}} \cdot \mathbf{b} \vec{\mathbf{m}} \quad (25)$$

and

$$\begin{aligned} \mathbb{E}[\vec{x}^T \mathbf{A} \vec{x} \cdot \mathbf{b} \vec{x}] &= \mathbf{b} \Sigma (\mathbf{A} + \mathbf{A}^T) \vec{\mathbf{m}} \\ &\quad + \text{Tr}(\Sigma \mathbf{A}^T) \mathbf{b} \vec{\mathbf{m}} + \mathbf{b} \vec{\mathbf{m}} \cdot \vec{\mathbf{m}}^T \mathbf{A} \vec{\mathbf{m}}. \end{aligned} \quad (26)$$

B. Mean and Variance

By again using standard matrix theory for quadratic and linear forms [17],

$$\mathbb{E}[\xi] = \mu_{\text{noise}} + \text{Tr}(\mathbf{A} \Sigma_{\vec{\mathbf{m}}}) + \mu_{\vec{\mathbf{m}}}^T \mathbf{A} \mu_{\vec{\mathbf{m}}} + \mathbf{b} \mu_{\vec{\mathbf{m}}}, \quad (27)$$

where $\Sigma_{\vec{\mathbf{m}}}$ is the covariance matrix of $\vec{\mathbf{m}}$ and $\mu_{\vec{\mathbf{m}}}$ is its mean vector. For random carrier phases, $\mu_{\vec{\mathbf{m}}} = \mathbf{0}$, so

$$\mathbb{E}[\xi] = \mu_{\text{noise}} + \text{Tr}(\mathbf{A} \Sigma_{\vec{\mathbf{m}}}), \quad (28)$$

where the covariance matrix $\Sigma_{\vec{\mathbf{m}}}$ is derived in (38). The unconditional variance is obtained with

$$\begin{aligned} \text{Var}[\xi] &= \text{Var}_{\text{noise}} + \text{Tr}(\mathbf{A}_2 \Sigma_{\vec{\mathbf{m}}}) + \mu_{\vec{\mathbf{m}}}^T \mathbf{A}_2 \mu_{\vec{\mathbf{m}}} \\ &\quad + \mathbf{b}_2 \mu_{\vec{\mathbf{m}}} + \text{Var}[\mathbb{E}[\xi | \vec{\mathbf{m}}]], \end{aligned} \quad (29)$$

where

$$\mathbf{A}_2 = (\mathbf{A} + \mathbf{A}^T) \Sigma (\mathbf{A} + \mathbf{A}^T) \quad (30)$$

and

$$\mathbf{b}_2 = 2\mathbf{b} \Sigma (\mathbf{A} + \mathbf{A}^T). \quad (31)$$

We assume random carrier phases, i.e., $\mu_{\vec{\mathbf{m}}} = \mathbf{0}$. Thus,

$$\text{Var}[\xi] = \text{Var}_{\text{noise}} + \text{Tr}(\mathbf{A}_2 \Sigma_{\vec{\mathbf{m}}}) + \text{Var}[\vec{\mathbf{m}}^T \mathbf{A} \vec{\mathbf{m}} + \mathbf{b} \vec{\mathbf{m}}], \quad (32)$$

where the first two terms in the right-hand-side can be directly evaluated but the last term requires more derivation.

C. Derivation of $\text{Var}[\vec{\mathbf{m}}^T \mathbf{A} \vec{\mathbf{m}} + \mathbf{b} \vec{\mathbf{m}}]$ in (32)

Herein, we derive the last term in (32). The randomness (and thus variance) in it is a result of the assumed random and independent carrier phases in signals. Given that there is an arbitrary number of signals M and given that signals affect each other, it is very challenging to derive the variance.

To attack this problem, we represent the Fourier series coefficients of a signal with carrier phase as a scalar multiplication of two matrix components in (35). This representation of signals with carrier phases is used in (39) to obtain alternative form of $\vec{\mathbf{m}}^T \mathbf{A} \vec{\mathbf{m}} + \mathbf{b} \vec{\mathbf{m}}$, which has carrier phases as scalar factors. By tedious expansion of the integrand in (44) to terms consisting of cosines and sines of random carrier phases, and by integrating each term, we finally obtain theoretically the variance in (45). It is valid for an arbitrary number of signals, each with an arbitrary waveform, time offset, and frequency offset.

We make the assumption that

$$F_{\text{PULSE}}(f) = 0, \quad |f| \geq f_c. \quad (33)$$

This assumption means that the baseband signal, when moved to the center frequency $\pm f_c$ is not extending to the other side. Thus, the baseband signal moved to f_c is not extending to negative frequencies. It also means that $c_0 = 0$. This assumption

is reasonable to assume since otherwise the signal is not a real passband signal.

By making this assumption, the carrier phase rotation can simply be represented by multiplication of the signal's complex Fourier series coefficients with $\exp(i\theta_i)$, where θ_i is the carrier phase of signal component i . It is easy to note that the result of this random carrier phase rotation on the real-valued Fourier-series coefficients is

$$\begin{aligned} a_n^{\text{ROT}} &= \cos(\theta) a_n + \sin(\theta) b_n \\ b_n^{\text{ROT}} &= -\sin(\theta) a_n + \cos(\theta) b_n, \end{aligned} \quad (34)$$

where $n = 1, 2, \dots, N$, a_n^{ROT} and b_n^{ROT} are the coefficients after carrier phase rotation and a_n and b_n are the coefficients before it. Due to the assumptions, $a_0 = 0$ and can thus be ignored.

Now, we take as input the sum of signal components in (16) and add a random carrier phase to each signal component following the result in (34). We get the signal components after random carrier phases with

$$\vec{\mathbf{m}} = \sum_{i=1}^M [\cos(\theta_i) \mathbf{A}_C E_{\text{rad},i} \vec{\mathbf{s}}_i + \sin(\theta_i) \mathbf{A}_S E_{\text{rad},i} \vec{\mathbf{s}}_i], \quad (35)$$

where an auxiliary $2N + 1 \times 2N + 1$ matrix

$$\mathbf{A}_C = \begin{bmatrix} 0 & 0_{1,N} & 0_{1,N} \\ 0_{N,1} & I_N & 0_N \\ 0_{N,1} & 0_N & I_N \end{bmatrix}, \quad (36)$$

where I_N is the $N \times N$ identity matrix and 0_N is the $N \times N$ zero matrix and another auxiliary matrix is

$$\mathbf{A}_S = \begin{bmatrix} 0 & 0_{1,N} & 0_{1,N} \\ 0_{N,1} & 0_N & I_N \\ 0_{N,1} & -I_N & 0_N \end{bmatrix}. \quad (37)$$

The covariance matrix for $\vec{\mathbf{m}}$ can be derived as

$$\Sigma_{\vec{\mathbf{m}}} = \sum_{i=1}^M \left[\frac{E_{\text{rad},i}^2}{2} \mathbf{A}_C \vec{\mathbf{s}}_i \vec{\mathbf{s}}_i^T \mathbf{A}_C^T + \frac{E_{\text{rad},i}^2}{2} \mathbf{A}_S \vec{\mathbf{s}}_i \vec{\mathbf{s}}_i^T \mathbf{A}_S^T \right]. \quad (38)$$

By using (35) in $\vec{\mathbf{m}}^T \mathbf{A} \vec{\mathbf{m}} + \mathbf{b} \vec{\mathbf{m}}$, we can represent it in terms of cosines/sines of the θ_i as

$$\begin{aligned} \vec{\mathbf{m}}^T \mathbf{A} \vec{\mathbf{m}} + \mathbf{b} \vec{\mathbf{m}} &= \sum_{i=1}^M \sum_{j=1}^M \cos(\theta_i) \cos(\theta_j) \nu_{i,j}^{cc} \\ &+ \sum_{i=1}^M \sum_{j=1}^M \cos(\theta_i) \sin(\theta_j) \nu_{i,j}^{cs} \\ &+ \sum_{i=1}^M \sum_{j=1}^M \sin(\theta_i) \cos(\theta_j) \nu_{i,j}^{sc} \\ &+ \sum_{i=1}^M \sum_{j=1}^M \sin(\theta_i) \sin(\theta_j) \nu_{i,j}^{ss} \\ &+ \sum_{k=1}^M \cos(\theta_k) \nu_k^c + \sum_{k=1}^M \sin(\theta_k) \nu_k^s, \end{aligned} \quad (39)$$

where constants

$$\begin{aligned} \nu_{i,j}^{cc} &= E_{\text{rad},i} E_{\text{rad},j} \vec{\mathbf{s}}_i^T \mathbf{A}_C^T \mathbf{A} \mathbf{A}_C \vec{\mathbf{s}}_j, \\ \nu_{i,j}^{cs} &= E_{\text{rad},i} E_{\text{rad},j} \vec{\mathbf{s}}_i^T \mathbf{A}_C^T \mathbf{A} \mathbf{A}_S \vec{\mathbf{s}}_j, \\ \nu_{i,j}^{sc} &= E_{\text{rad},i} E_{\text{rad},j} \vec{\mathbf{s}}_i^T \mathbf{A}_S^T \mathbf{A} \mathbf{A}_C \vec{\mathbf{s}}_j, \\ \nu_{i,j}^{ss} &= E_{\text{rad},i} E_{\text{rad},j} \vec{\mathbf{s}}_i^T \mathbf{A}_S^T \mathbf{A} \mathbf{A}_S \vec{\mathbf{s}}_j, \\ \nu_k^c &= E_{\text{rad},k} \mathbf{b} \mathbf{A}_C \vec{\mathbf{s}}_k, \\ \nu_k^s &= E_{\text{rad},k} \mathbf{b} \mathbf{A}_S \vec{\mathbf{s}}_k. \end{aligned} \quad (40)$$

Let us collect the uniformly distributed phases in a vector

$$\boldsymbol{\theta} = [\theta_1 \quad \theta_2 \quad \dots \quad \theta_M], \quad (41)$$

which has the probability density function

$$f(\boldsymbol{\theta}) = \begin{cases} \left(\frac{1}{2\pi}\right)^M & 0 \leq \theta_i < 2\pi, \forall_i \\ 0 & \text{otherwise.} \end{cases} \quad (42)$$

By using (39) and (42), we straightforwardly get

$$\begin{aligned} \mathbb{E} [\vec{\mathbf{m}}^T \mathbf{A} \vec{\mathbf{m}} + \mathbf{b} \vec{\mathbf{m}}] &= \int \left(\vec{\mathbf{m}}^T \mathbf{A} \vec{\mathbf{m}} + \mathbf{b} \vec{\mathbf{m}} \right) \cdot f(\boldsymbol{\theta}) d\boldsymbol{\theta} \\ &= \sum_{i=1}^M \frac{\nu_{i,i}^{cc} + \nu_{i,i}^{ss}}{2}. \end{aligned} \quad (43)$$

To get variance, we use (39) and (42) and find

$$\begin{aligned} \mathbb{E} \left[\left(\vec{\mathbf{m}}^T \mathbf{A} \vec{\mathbf{m}} + \mathbf{b} \vec{\mathbf{m}} \right)^2 \right] &= \int \left(\vec{\mathbf{m}}^T \mathbf{A} \vec{\mathbf{m}} + \mathbf{b} \vec{\mathbf{m}} \right)^2 \cdot f(\boldsymbol{\theta}) d\boldsymbol{\theta}, \end{aligned} \quad (44)$$

where we expand $(\vec{\mathbf{m}}^T \mathbf{A} \vec{\mathbf{m}} + \mathbf{b} \vec{\mathbf{m}}) \cdot (\vec{\mathbf{m}}^T \mathbf{A} \vec{\mathbf{m}} + \mathbf{b} \vec{\mathbf{m}})$ to get terms consisting of product cosine/sine terms which are easy to integrate. Finally, we get

$$\begin{aligned} \text{Var} \left[\vec{\mathbf{m}}^T \mathbf{A} \vec{\mathbf{m}} + \mathbf{b} \vec{\mathbf{m}} \right] &= \frac{1}{8} \sum_{i=1}^M \left[(\nu_{i,i}^{cc})^2 + (\nu_{i,i}^{ss})^2 + (\nu_{i,i}^{cs})^2 + (\nu_{i,i}^{sc})^2 \right] \\ &+ \frac{1}{2} \sum_{i=1}^M \left((\nu_i^c)^2 + (\nu_i^s)^2 + \frac{\nu_{i,i}^{cs} \nu_{i,i}^{sc}}{2} - \frac{\nu_{i,i}^{cc} \nu_{i,i}^{ss}}{2} \right) \\ &+ \frac{1}{4} \sum_{i=1}^M \sum_{j=1, j \neq i}^M \left((\nu_{i,j}^{cc})^2 + (\nu_{i,j}^{cs})^2 + (\nu_{i,j}^{sc})^2 + (\nu_{i,j}^{ss})^2 \right) \\ &+ \frac{1}{2} \sum_{i=1}^M \sum_{j=i+1}^M \left(\nu_{i,j}^{cc} \nu_{j,i}^{cc} + \nu_{i,j}^{cs} \nu_{j,i}^{sc} + \nu_{i,j}^{sc} \nu_{j,i}^{cs} + \nu_{i,j}^{ss} \nu_{j,i}^{ss} \right), \end{aligned} \quad (45)$$

where we can notice that only the terms where each cosine or sine of phase present in the term is repeated two or four times. For example, the term involving $\nu_{i,j}^{cs} \nu_{j,i}^{sc}$ has the cosine of phase θ_i two times and sine of phase θ_j two times, according to the expansion (39). As another example, the term involving $(\nu_{i,i}^{ss})^2$ has the sine of phase θ_i four times. The reason is that individual cosine or sine terms of a phase will lead to integration result zero.

V. BIT ERROR PROBABILITY WITH GAUSSIAN APPROXIMATION

Following [9], thresholding with threshold η is used for the average-level detector output so that $\varepsilon < \eta$ corresponds to bit 1 and $\varepsilon \geq \eta$ corresponds to bit 0. We assume $M_T - 1$ interfering signal sources (which can be on or off depending on their current bit, so the number of current active signals M varies from 0 to M_T). The BEP is then

$$P_E = \frac{1}{2^{M_T}} \sum_{\Omega \in \{0,1\}^{M_T-1}} \text{Prob}(\xi < \eta | b_1 = 0 \& b_{2:M_T} = \Omega) \\ + \frac{1}{2^{M_T}} \sum_{\Omega \in \{0,1\}^{M_T-1}} \text{Prob}(\xi \geq \eta | b_1 = 1 \& b_{2:M_T} = \Omega) \quad (46)$$

where b_1 is the bit of the considered transmitter and vector Ω contains the states b_2, b_3, \dots, b_{M_T} of the interfering signals. All possible states are assumed to be equally likely. By invoking the Gaussian-mixture approximation,

$$P_E \approx \frac{1}{2^{M_T}} \sum_{\Omega \in \{0,1\}^{M_T-1}} \Phi \left(\frac{\eta - \mathbb{E}_{b_1=0, b_{2:M_T}=\Omega}}{\sqrt{\text{Var}_{b_1=0, b_{2:M_T}=\Omega}}} \right) \\ + \frac{1}{2^{M_T}} \sum_{\Omega \in \{0,1\}^{M_T-1}} Q_{\text{func}} \left(\frac{\eta - \mathbb{E}_{b_1=1, b_{2:M_T}=\Omega}}{\sqrt{\text{Var}_{b_1=1, b_{2:M_T}=\Omega}}} \right), \quad (47)$$

where Φ is the normal cumulative distribution function and Q_{func} is the Q -function and, for example, $\mathbb{E}_{b_1=0, b_{2:M_T}=\Omega}$ denotes the mean for the given states of the transmitters (which lead to the number of active signals M).

VI. NUMERICAL RESULTS

First, we present the pulse shapes used for numerical results. The numerical results show the effects of co-channel interference, adjacent channel interference, and ISI. The BEPs are found using (47) with means and variances found in Section IV. From the results we see the required spatial separation, frequency separation, and additional guard time needed in order to not significantly degrade BEP compared to case without interference.

A. Pulse Shapes $p(t)$

In practical on-off keying radios, sharp power level transitions, such as with the previously considered rectangular pulse are undesired due to spectral widening [18]. This the reason for considering more general trapezoidal pulse and the Hanning pulse, which have reduced spectral widening.

The average energy per bit is $TP/2$, where P is the average transmit power during pulse (on, bit 1). In all of the following results we assume that transmit power P is selected so that the average energy per bit at the transmitter is 10 nJ (nanojoules).

1) *Trapezoidal Pulse*: The trapezoidal pulse is (with unit average power during the pulse duration)

$$p(t) = \sqrt{\frac{T}{T - \frac{4}{3}\tau_{\text{rise}}}} \times \begin{cases} t/\tau_{\text{rise}} & 0 \leq t < \tau_{\text{rise}} \\ 1 & \tau_{\text{rise}} \leq t < T - \tau_{\text{rise}} \\ T - t & T - \tau_{\text{rise}} \leq t < T \\ 0 & \text{otherwise} \end{cases} \quad (48)$$

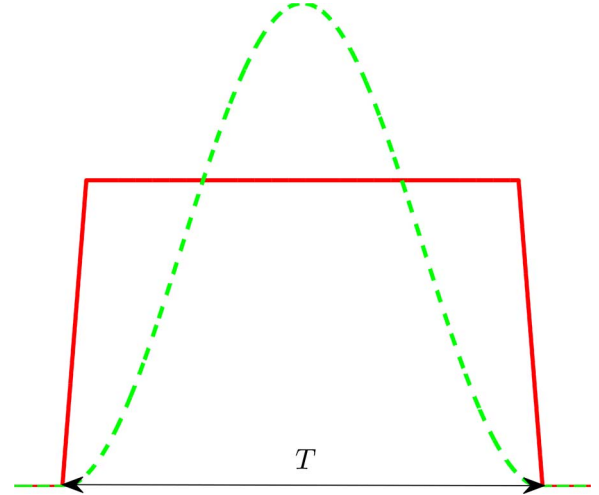


Fig. 3. Trapezoidal (red solid line), and Hanning (green dashed line) pulses $p(t)$, pulse duration T and equal average power during pulse duration.

where, following recommendations in [18], we assume $\tau_{\text{rise}} = \frac{T}{20}$. Please note that $\tau_{\text{rise}} = 0$ would correspond to the rectangular pulse and $\tau_{\text{rise}} = T/2$ would correspond to the triangular pulse shape. The Fourier transform of the trapezoidal pulse at frequency f is

$$F_{\text{PULSE, trapez}}(f) = (T - \tau_{\text{rise}}) \text{sinc}(f(T - \tau_{\text{rise}})) \\ \cdot \text{sinc}(f\tau_{\text{rise}}) \exp(-i\pi T f) \cdot \sqrt{\frac{T}{T - \frac{4}{3}\tau_{\text{rise}}}} \quad (49)$$

where

$$\text{sinc}(x) = \begin{cases} 1 & x = 0 \\ \frac{\sin(\pi x)}{\pi x} & \text{otherwise.} \end{cases} \quad (50)$$

2) *Hanning Pulse*: The Hanning pulse with unit average power during pulse duration is

$$p(t) = \begin{cases} \sqrt{(8/3)} \cdot \frac{1}{2} \left[1 + \cos\left(\frac{2\pi(t-T/2)}{T}\right) \right] & 0 \leq t \leq T \\ 0 & \text{otherwise.} \end{cases} \quad (51)$$

Its Fourier transform is

$$F_{\text{PULSE, Hanning}}(f) = \sqrt{(8/3)} \\ \cdot \frac{T}{2} \left(\text{sinc}(fT) + \frac{1}{2}\text{sinc}(fT - 1) \right) \\ + \frac{1}{2}\text{sinc}(fT + 1) \exp(-i\pi T f). \quad (52)$$

Fig. 3 illustrates the above pulse shapes in the time domain. Since these pulses are zero outside the interval $0 \leq t \leq T_P$ (where $T_P \geq T$), the complex Fourier series coefficients for the time interval $t \in [0, T_P]$ are obtained with (6).

B. Performance Under Interference

In all of the following results, we have used integration windows which have been optimized when interference is not present. Optimization of integration window at run-time taking into account interfering signals with minimal complexity is an interesting and very challenging problem for future work. The optimal integration window is almost constant for different signal powers when interference is not present, so luckily the

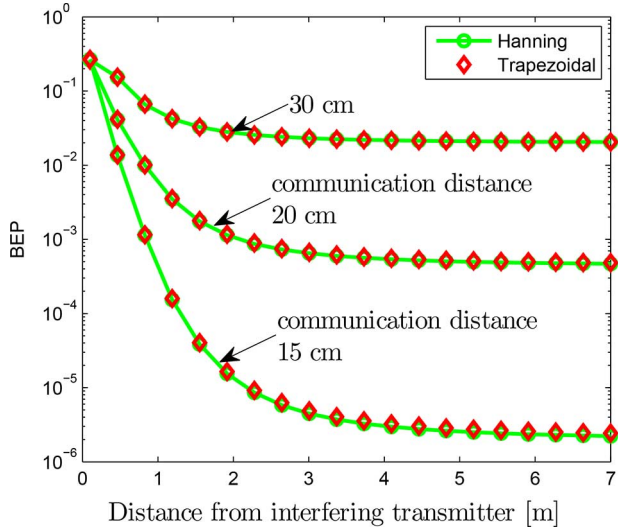


Fig. 4. Bit error probability with co-channel interference, resonance frequency and carrier frequency 82 MHz, quality factor $Q = 800$. Pulse duration $T = 7.2532 \mu\text{s}$, average bit energy 10 nJ.

receiver does not need to estimate the signal power for setting the integration window. The optimal detection threshold η (to determine if the observed decision statistic corresponds to bit 0 or 1) has been assumed in all cases, it can be obtained through, for example, training sequences or adaptive algorithms (also left for future work).

In all the following results, the pulse duration $T = 7.2532 \mu\text{s}$, and the integration window $[\epsilon T_{\text{int}} + \epsilon]$ to be used in (19) for Hanning pulse (normalized by T) is $[0.50691 \ 0.96256]$ and integration window for Trapezoidal pulse (normalized by T) is $[0.37748 \ 1.16267]$.

1) *Co-Channel Interference*: Fig. 4 shows the BEP with an interfering transmitter in the same frequency when the distance from the interfering transmitter is varied. The interfering transmitter is assumed to use exactly the same parameters as the considered transmitter and it also uses on-off keying. Results assume the worst case where both transmitters have the same bit intervals, i.e., pulses start at the same time. It can be seen from Fig. 4 that for communication links with 15, 20, and 30 cm link distances, the required spatial separation from an interfering transmitter to get performance close to no-interference is several meters. Thus, the co-channel interference has a significant effect on BEP and does not depend on the pulse shape.

2) *Adjacent Channel Interference*: Fig. 5 shows the BEP with adjacent channel interference simultaneously from both the channel above and the channel below the considered channel when the channel separation Δf is varied as illustrated in Fig. 2. It can be seen that with a small frequency separation values trapezoidal pulse has better performance. This is due to a smaller main lobe width as compared to the Hanning pulse. However, at larger values performances are equal. The BEP with trapezoidal pulse fluctuates due strong sidelobes, when a strong sidelobe affects the studied channel its BEP gets worse.

In addition to the theoretical results using the Gaussian approximation, computer simulations were performed using high oversampling to accurately approximate the continuous time

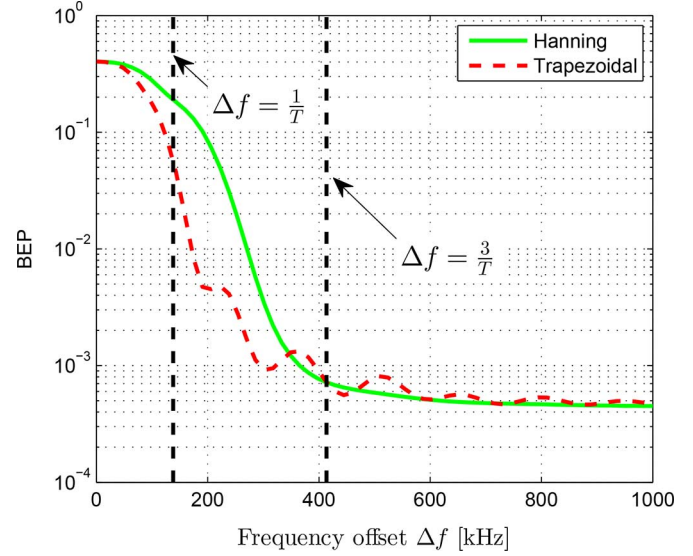


Fig. 5. Bit error probability with adjacent channel interference, resonance frequency and carrier frequency 82 MHz, quality factor $Q = 800$. Pulse duration $T = 7.2532 \mu\text{s}$, average bit energy 10 nJ. Communication distance and distance from interfering transmitter both equal to 20 cm.

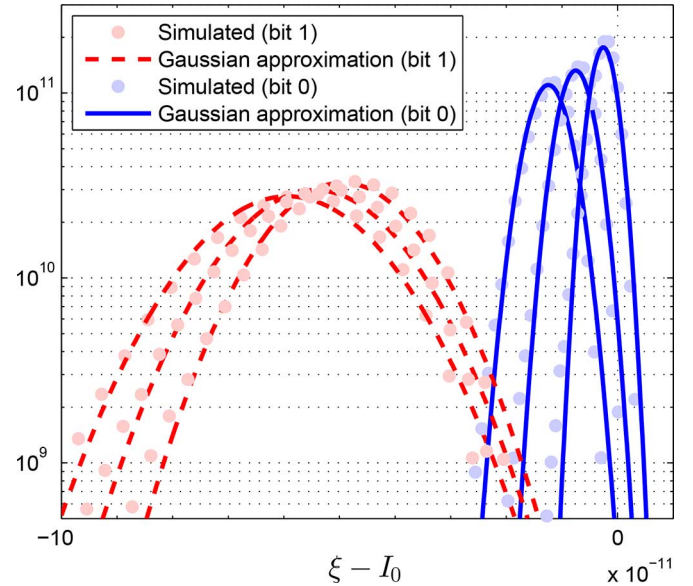


Fig. 6. Probability density function of the decision statistic with adjacent channel interference, $\Delta f = 200$ kHz, resonance frequency and carrier frequency 82 MHz, quality factor $Q = 800$. Pulse duration $T = 7.2532 \mu\text{s}$, average bit energy 10 nJ. Communication distance and distance from interfering transmitter both equal to 20 cm.

radio frequency signals (with random carrier phases) and colored noise in (14), transfer function of the CNT (7), the mapping to output current (18), and the calculation of the decision statistic (19). Simulation results and results from the Gaussian approximation are shown in Fig. 6 for the case with adjacent channel interference. The results are shown for the cases when the studied bit is 1 or 0 and the interfering signals (from channels above and below) are on or off. There are 4 possibilities for interfering signals to be on or off (however two of these possibilities lead to equivalent results so only 3 cases are visible). We observe good agreement with the simulated and theoretical

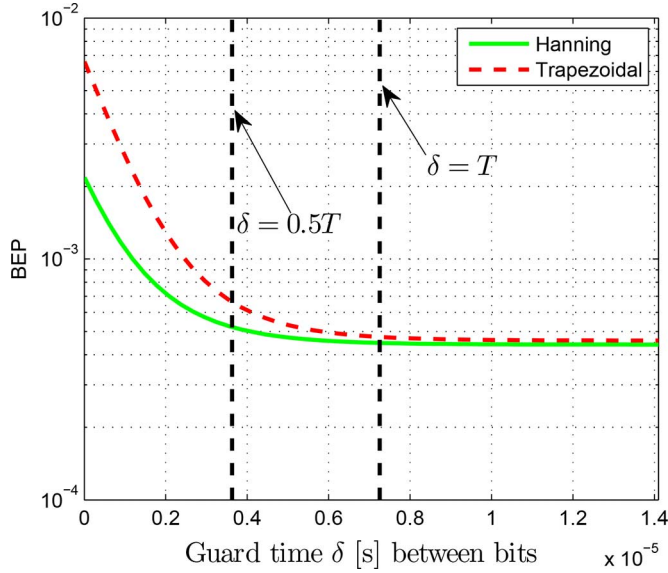


Fig. 7. Bit error probability with inter symbol interference when additional guard time δ between pulses is varied, resonance frequency and carrier frequency 82 MHz, quality factor $Q = 200$. Pulse duration $T = 7.2532 \mu\text{s}$ (0.72532×10^{-5}), average bit energy 10 nJ. Communication distance 20 cm.

results, with some differences in tails. We emphasize that the theoretical mean and variance are exact and the difference in tails is due to the Gaussian approximation. For more accuracy for tails distributions, generalized Gaussian distributions can be used. However, they require more input parameters than just the mean and variance. As the Gaussian approximation is used in all papers for nanoscale VHF-band communications, finding distributions with better fitting in the tails and not requiring difficult to find input parameters is an important open research problem for future work.

3) *Inter Symbol Interference*: Fig. 7 shows the BEP with inter symbol interference when additional guard time δ (in addition to T) is varied, see Fig. 2 for illustration. It can be seen that with a small guard time, the Hanning pulse has better performance. This is due to a more focused pulse leading to a shorter response after the CNT filter, and also due to shorter optimal integration window under the no-interference case.

VII. CONCLUSION

A framework for analysis of nanonetworks with CNT based reception under many practical effects such as transient components has been presented. The objective of this work is to study performance of nanoscale CNT based wireless communication under interference. Theoretical results are derived for mean and variance of the average-level detector output under an arbitrary number interfering signals. The results are used to obtain bit error probability (BEP) expressions with the Gaussian approximation. The results demonstrate that co-channel interference can seriously degrade the performance of nanonetworks, but the adjacent channel interference and ISI can be suppressed with the proper selection of frequency separation between channels and additional guard time between pulses. Although there are still several interesting open questions for future work, e.g., those mentioned in this paper, the results confirm the CNT based com-

munication in the VHF-band as a promising paradigm for wireless communication in nanoscale.

APPENDIX A

To derive the covariance matrix Σ of vector of Fourier series coefficients of the thermomechanical noise, we first note that

$$\begin{aligned} \mathbb{E}[a_n b_k] &= \frac{4}{T_P^2} \int_{x=0}^{T_P} \int_{t=0}^{T_P} C_{y_{\text{noise}}}(t-x) \\ &\quad \times \cos\left(\frac{2\pi n x}{T_P}\right) \sin\left(\frac{2\pi n t}{T_P}\right) dx dt = 0 \end{aligned}$$

so that a_n and b_n are independent. To get the covariance for the cosine terms, we evaluate

$$\begin{aligned} \mathbb{E}[a_n a_k] &= \frac{4}{T_P^2} \int_{x=0}^{T_P} \int_{t=0}^{T_P} C_{y_{\text{noise}}}(t-x) \\ &\quad \times \cos\left(\frac{2\pi n x}{T_P}\right) \cos\left(\frac{2\pi k t}{T_P}\right) dx dt, \end{aligned}$$

which, by performing the integration, leads to

$$\begin{aligned} \mathbb{E}[a_n a_k] &= \frac{4}{T_P^2} \cdot \begin{cases} \frac{T_P^3 \bar{\omega}}{(T_P^2 v^2 + 4\pi^2 n^2)(u-v)} \\ - \frac{T_P^3 \bar{\omega}}{(T_P^2 u^2 + 4\pi^2 n^2)(u-v)} \\ + \frac{2T_P^4 u \bar{\omega} e^{-T_P u} (e^{T_P u} - 1)}{(T_P^2 u^2 + 4\pi^2 n^2)^2 (u-v)} \\ - \frac{2T_P^4 v \bar{\omega} e^{-T_P v} (e^{T_P v} - 1)}{(T_P^2 v^2 + 4\pi^2 n^2)^2 (u-v)} \\ - \frac{2T_P^4 u \bar{\omega} e^{-T_P u} (e^{T_P u} - 1)}{(T_P^2 u^2 + 4\pi^2 k^2)(T_P^2 u^2 + 4\pi^2 n^2) m u (u-v)} \\ - \frac{2T_P^4 v \bar{\omega} e^{-T_P v} (e^{T_P v} - 1)}{(T_P^2 v^2 + 4\pi^2 k^2)(T_P^2 v^2 + 4\pi^2 n^2)(u-v)} \end{cases} & k = n \\ & & k \neq n \end{aligned}$$

where $\bar{\omega} = \frac{k_B T_K}{m_{\text{eff}}}$. Similarly for the sinusoidal terms we obtain

$$\begin{aligned} \mathbb{E}[b_n b_k] &= \frac{4}{T_P^2} \cdot \begin{cases} \frac{T_P^3 \bar{\omega}}{(T_P^2 v^2 + 4\pi^2 n^2)(u-v)} \\ - \frac{T_P^3 \bar{\omega}}{(T_P^2 u^2 + 4\pi^2 n^2)(u-v)} \\ - \frac{8T_P^2 \pi^2 n^2 \bar{\omega} e^{-T_P u} (e^{T_P u} - 1)}{u(T_P^2 u^2 + 4\pi^2 n^2)^2 (u-v)} \\ + \frac{8T_P^2 \pi^2 n^2 \bar{\omega} e^{-T_P v} (e^{T_P v} - 1)}{v(T_P^2 v^2 + 4\pi^2 n^2)^2 (u-v)} \\ + \frac{8T_P^2 \pi^2 k n \bar{\omega} e^{-T_P u} (e^{T_P u} - 1)}{v(T_P^2 v^2 + 4\pi^2 k^2)(T_P^2 v^2 + 4\pi^2 n^2)(u-v)} \\ - \frac{8T_P^2 \pi^2 k n \bar{\omega} e^{-T_P v} (e^{T_P v} - 1)}{u(T_P^2 u^2 + 4\pi^2 k^2)(T_P^2 u^2 + 4\pi^2 n^2)(u-v)} \end{cases} & k = n \\ & & k \neq n \end{aligned}$$

Finally, we obtain the full $(2N + 1) \times (2N + 1)$ covariance matrix as

$$\Sigma = \begin{bmatrix} \mathbb{E}[a_n a_k]_{k,n \in \{0,1,\dots,N\}} & \mathbf{0} \\ \mathbf{0} & \mathbb{E}[b_n b_k]_{k,n \in \{1,2,\dots,N\}} \end{bmatrix}.$$

APPENDIX B

Let us write the decision statistic (19) as

$$\xi = \xi_2 + \xi_1 + I_0, \quad (53)$$

where

$$\xi_2 = \frac{I_0 \alpha_2}{T_{\text{int}}} \int_{t=\epsilon}^{T_{\text{int}}+\epsilon} y(t)^2 dt, \quad (54)$$

and

$$\xi_1 = \frac{I_0 \alpha_1}{T_{\text{int}}} \int_{t=\epsilon}^{T_{\text{int}}+\epsilon} y(t) dt. \quad (55)$$

For theoretical analysis, we find a matrix theoretical representation of the decision statistic (53). We do this by separately considering the square-law component ξ_2 and the linear component ξ_1 .

The matrix representation is obtained by using the Fourier series representation (1) of the input $y(t)$ in $t \in [0 T_P]$ and by using the Fourier series coefficients collected into a vector as in (2). The input $y(t)$ includes thermomechanical noise and all signals present. By using Fourier representation of the input $y(t)$, $t \in [0 T_P]$ in (1) and plugging into (54), we get

$$\xi_2 = \frac{I_0 \alpha_2}{T_{\text{int}}} \int_{t=\epsilon}^{T_{\text{int}}+\epsilon} \left[\frac{a_0}{2} + \sum_{n=1}^N \begin{pmatrix} a_n \cos\left(\frac{2\pi n t}{T_P}\right) \\ + b_n \sin\left(\frac{2\pi n t}{T_P}\right) \end{pmatrix} \right]^2 dt. \quad (56)$$

By expanding the terms due to squaring, and performing integration on each term, we find that the result can be represented as a quadratic form

$$\xi_2 = \bar{\mathbf{x}}^T \mathbf{A} \bar{\mathbf{x}}, \quad (57)$$

where $\bar{\mathbf{x}}$ is given in (15) and the matrix \mathbf{A} is derived in the Appendix C. The linear component is

$$\begin{aligned} \xi_1 &= \frac{I_0 \alpha_1}{T_{\text{int}}} \int_{t=\epsilon}^{T_{\text{int}}+\epsilon} \left(\frac{a_0}{2} + \sum_{n=1}^N \begin{pmatrix} a_n \cos\left(\frac{2\pi n t}{T_P}\right) \\ + b_n \sin\left(\frac{2\pi n t}{T_P}\right) \end{pmatrix} \right) dt \\ &= \mathbf{b} \bar{\mathbf{x}}, \end{aligned} \quad (58)$$

where the vector \mathbf{b} is derived in the Appendix C.

By summing the square-law, linear, and constant components, we finally get the result in (20).

APPENDIX C

The matrix \mathbf{A} is

$$\begin{aligned} \mathbf{A} &= \frac{I_0 \alpha_2}{T_{\text{int}}} \\ &\times \begin{bmatrix} \frac{1}{4} T_{\text{int}} & \frac{1}{2} \mathbf{v}_{\mathbf{c}}(N, T_{\text{int}}, T_P) & \frac{1}{2} \mathbf{v}_{\mathbf{s}}(N, T_{\text{int}}, T_P) \\ \frac{1}{2} \mathbf{v}_{\mathbf{c}}(N, T_{\text{int}}, T_P)^T & \mathbf{m}_{\mathbf{cc}}(N, T_{\text{int}}, T_P) & \mathbf{m}_{\mathbf{cs}}(N, T_{\text{int}}, T_P) \\ \frac{1}{2} \mathbf{v}_{\mathbf{s}}(N, T_{\text{int}}, T_P)^T & \mathbf{m}_{\mathbf{cs}}(N, T_{\text{int}}, T_P)^T & \mathbf{m}_{\mathbf{ss}}(N, T_{\text{int}}, T_P) \end{bmatrix} \end{aligned}$$

where row vector

$$\begin{aligned} \mathbf{v}_{\mathbf{c}}(N, T_{\text{int}}, T_P) &= \left[\frac{T_P \left(\sin\left(\frac{2\pi n (T_{\text{int}}+\epsilon)}{T_P}\right) - \sin\left(\frac{2\pi n \epsilon}{T_P}\right) \right)}{2\pi n} \right]_{n=1,2,\dots,N} \end{aligned}$$

and row vector

$$\begin{aligned} \mathbf{v}_{\mathbf{s}}(N, T_{\text{int}}, T_P) &= \left[-\frac{T_P \left(\cos\left(\frac{2\pi n (T_{\text{int}}+\epsilon)}{T_P}\right) - \cos\left(\frac{2\pi n \epsilon}{T_P}\right) \right)}{2\pi n} \right]_{n=1,2,\dots,N} \end{aligned}$$

and $N \times N$ matrix ($k = 1, \dots, N$ and $j = 1, \dots, N$)

$$\begin{aligned} \mathbf{m}_{\mathbf{cc}}(N, T_{\text{int}}, T_P) &= \begin{cases} \frac{T_{\text{int}}}{2} + \frac{\left(\frac{T_P \sin\left(\frac{4\pi n (T_{\text{int}}+\epsilon)}{T_P}\right)}{8} - \frac{T_P \sin\left(\frac{4\pi n \epsilon}{T_P}\right)}{8} \right)}{\pi n} & k = n \\ \frac{T_P \sin\left(\frac{2\pi (T_{\text{int}}+\epsilon)(k+n)}{T_P}\right)}{4\pi(k+n)} - \frac{T_P \sin\left(\frac{2\pi \epsilon(k-n)}{T_P}\right)}{4\pi(k-n)} & \\ -\frac{T_P \sin\left(\frac{2\pi \epsilon(k+n)}{T_P}\right)}{4\pi(k+n)} + \frac{T_P \sin\left(\frac{2\pi (T_{\text{int}}+\epsilon)(k-n)}{T_P}\right)}{4\pi(k-n)} & k \neq n \end{cases} \end{aligned}$$

and $N \times N$ matrix

$$\begin{aligned} \mathbf{m}_{\mathbf{ss}}(N, T_{\text{int}}, T_P) &= \begin{cases} \frac{T_{\text{int}}}{2} - \frac{\left(\frac{T_P \sin\left(\frac{4\pi n (T_{\text{int}}+\epsilon)}{T_P}\right)}{8} - \frac{T_P \sin\left(\frac{4\pi n \epsilon}{T_P}\right)}{8} \right)}{\pi n} & k = n \\ \frac{T_P \sin\left(\frac{2\pi \epsilon(k+n)}{T_P}\right)}{4\pi(k+n)} - \frac{T_P \sin\left(\frac{2\pi \epsilon(k-n)}{T_P}\right)}{4\pi(k-n)} & \\ \frac{T_P \sin\left(\frac{2\pi (T_{\text{int}}+\epsilon)(k-n)}{T_P}\right)}{4\pi(k-n)} - \frac{T_P \sin\left(\frac{2\pi (T_{\text{int}}+\epsilon)(k+n)}{T_P}\right)}{4\pi(k+n)} & k \neq n \end{cases} \end{aligned}$$

and $N \times N$ matrix

$$\begin{aligned} \mathbf{m}_{\mathbf{cs}}(N, T_{\text{int}}, T_P) &= \begin{cases} -\frac{T_P \left(\cos\left(\frac{4\pi n (T_{\text{int}}+\epsilon)}{T_P}\right) - \cos\left(\frac{4\pi n \epsilon}{T_P}\right) \right)}{8\pi n} & k = n \\ \frac{T_P \cos\left(\frac{2\pi \epsilon(k-n)}{T_P}\right)}{4\pi(k-n)} - \frac{T_P \cos\left(\frac{2\pi (T_{\text{int}}+\epsilon)(k+n)}{T_P}\right)}{4\pi(k+n)} & \\ +\frac{T_P \cos\left(\frac{2\pi \epsilon(k+n)}{T_P}\right)}{4\pi(k+n)} - \frac{T_P \cos\left(\frac{2\pi (T_{\text{int}}+\epsilon)(k-n)}{T_P}\right)}{4\pi(k-n)} & k \neq n \end{cases} \end{aligned}$$

The vector \mathbf{b} is

$$\mathbf{b} = \frac{I_0 \alpha_1}{T_{\text{int}}} \left[\frac{1}{2} T_{\text{int}} \quad \mathbf{v}_{\mathbf{c}}(N, T_{\text{int}}, T_P) \quad \mathbf{v}_{\mathbf{s}}(N, T_{\text{int}}, T_P) \right].$$

ACKNOWLEDGMENT

Prof. Markku Juntti is thanked for his comments which helped to improve the quality of the paper.

REFERENCES

- [1] J. Yao, H. Yan, S. Das, J. F. Klemic, J. C. Ellenbogen, and C. M. Lieber, "Nanowire nanocomputer as a finite-state machine," *Proc. Nat. Acad. Sci.*, vol. 111, no. 7, pp. 2431–2435, 2014.
- [2] I. F. Akyildiz and J. M. Jornet, "Electromagnetic wireless nanosensor networks," *Nano Commun. Netw. (Elsevier)*, vol. 1, no. 1, pp. 3–19, Mar. 2010.
- [3] S. Mohrehkesh and M. C. Weigle, "Optimizing energy consumption in terahertz band nanonetworks," *IEEE J. Sel. Areas Commun.*, vol. 32, no. 12, pp. 2432–2441, Dec. 2014.
- [4] J. M. Jornet and I. F. Akyildiz, "Femtosecond-long pulse-based modulation for terahertz band communication in nanonetworks," *IEEE Trans. Commun.*, vol. 62, no. 5, pp. 1742–1754, May 2014.
- [5] M. Kuscü, A. Kiraz, and O. B. Akan, "Fluorescent molecules as transceiver nanoantennas: The first practical and high-rate information transfer over a nanoscale communication channel based on FRET," *Nature Scientif. Rep.*, vol. 5, pp. 1–6, Jan. 2015, doi: 10.1038/srep07831; Article No. 7831 [Online]. Available: <http://www.nature.com/articles/srep07831>.
- [6] K. Jensen, J. Weldon, H. Garcia, and A. Zettl, "Nanotube radio," *Nano Lett.*, vol. 7, no. 11, pp. 3508–3511, Nov. 2007.

- [7] C. E. Koksal and E. Ekici, "A nanoradio architecture for interacting nanonetworking tasks," *Nano Commun. Netw. (Elsevier)*, vol. 1, no. 1, pp. 63–75, Mar. 2010.
- [8] C. E. Koksal, E. Ekici, and S. Rajan, "Design and analysis of systems based on RF receivers with multiple carbon nanotube antennas," *Nano Commun. Netw. (Elsevier)*, vol. 1, no. 3, pp. 160–172, Sept. 2010.
- [9] J. Lehtomäki, A. O. Bicen, and I. F. Akyildiz, "On the nanoscale electromechanical wireless communication in the VHF band," *IEEE Trans. Commun.*, vol. 63, pp. 311–323, Jan. 2015.
- [10] C. H. Lee, S. W. Lee, and S. S. Lee, "A nanoradio utilizing the mechanical resonance of a vertically aligned nanopillar array," *Nanoscale*, vol. 6, pp. 2087–2093, 2014.
- [11] L. Stoica, "Non-coherent energy detection transceivers for ultra wide-band impulse radio systems," Ph.D. dissertation, Univ. of Oulu, Oulu, Finland, 2008.
- [12] V. Niemelä, J. Haapola, M. Hämäläinen, and J. Iinatti, "Integration interval and threshold evaluation for an energy detector receiver with PPM and OOK modulation," in *Proc. BodyNets*, 2012, pp. 242–248 [Online]. Available: <http://dl.acm.org/citation.cfm?id=2442747>
- [13] T.-A. Phan, J. Lee, V. Krizhanovskii, S.-K. Han, and S.-G. Lee, "A 18-pJ/Pulse OOK CMOS transmitter for multiband UWB impulse radio," *IEEE Microw. Wireless Compon. Lett.*, vol. 17, no. 9, pp. 688–690, Sep. 2007.
- [14] R. C. Dorf and R. J. Tallarida, *Pocket Book of Electrical Engineering Formulas*. Boca Raton, FL, USA: CRC Press, 1993.
- [15] T. R. Albrecht, P. Grutter, D. Horne, and D. Rugar, "Frequency modulation detection using high-Q cantilevers for enhanced force microscope sensitivity," *J. Appl. Phys.*, vol. 69, no. 2, pp. 668–673, 1991.
- [16] P. Vincent *et al.*, "Performance of field-emitting resonating carbon nanotubes as radio-frequency demodulators," *Phys. Rev. B*, vol. 83, no. 15, Apr. 2011.
- [17] K. B. Petersen and M. S. Pedersen, *The Matrix Cookbook* Nov. 2012 [Online]. Available: <http://www2.imm.dtu.dk/pubdb/p.php?3274>
- [18] Infineon Technologies AG, "Usage of the TDK51xx/TDA71xx transmitters in the 868 MHz ISM band," May 2012 [Online]. Available: http://www.infineon.com/dgdl/TDK51xx_TDA71xx_AN_868MHz_ETSI_V1.0.pdf?fileId=db3a3043382e837301384bd2_416f435c



Janne J. Lehtomäki (S'03–M'06) got his doctorate in wireless communications from the University of Oulu, Finland, in 2005. Currently, he is a senior research fellow at the University of Oulu, Centre for Wireless Communications. He spent the fall 2013 semester at the Georgia Institute of Technology, Atlanta, USA, as a visiting scholar. Dr. Lehtomäki co-authored the paper receiving the Best Paper Award in IEEE WCNC 2012. He was the TPC co-chair for IWSS Workshop at IEEE WCNC 2015 and at IEEE WCNC 2016 and publicity co-chair for

ACM NANOCOM 2015 and publication chair for ACM NANOCOM 2016. Dr. Lehtomäki has served as a guest associate editor for two *IEICE Transactions on Communications* Special Sections, and as a managing guest editor for *Nano Communication Networks* (Elsevier) Special Issue EMCOM. He is an editorial board member of *Physical Communication* (Elsevier). Currently, he is focusing on nanonetworks, terahertz band communication, and dynamic spectrum access and cognitive radios.



A. Ozan Bicen (S'08) received the B.Sc. and M.Sc. degrees in electrical and electronics engineering from Middle East Technical University, Ankara, Turkey, in 2010 and from Koc University, Istanbul, Turkey in 2012, respectively. He is currently a Graduate Research Assistant in the Broadband Wireless Networking Laboratory and pursuing his Ph.D. degree at the School of Electrical and Computer Engineering, Georgia Institute of Technology, Atlanta, GA. His current research interests include molecular communication and nanonetworks.



Ian F. Akyildiz (M'86–SM'89–F'96) received the B.S., M.S., and Ph.D. degrees in computer engineering from the University of Erlangen-Nürnberg, Germany, in 1978, 1981 and 1984, respectively. Currently, he is the Ken Byers Chair Professor in Telecommunications with the School of Electrical and Computer Engineering, Georgia Institute of Technology, Atlanta, the Director of the Broadband Wireless Networking Laboratory and Chair of the Telecommunication Group at Georgia Tech. Dr. Akyildiz is an honorary professor with the School of Electrical Engineering at Universitat Politècnica de Catalunya (UPC) in Barcelona, Catalunya, Spain, and founded the N3Cat (NaNoNetworking Center in Catalunya). Since September 2012, Dr. Akyildiz is also a FiDiPro Professor (Finland Distinguished Professor Program (FiDiPro) supported by the Academy of Finland) at Tampere University of Technology, Department of Communications Engineering, Finland. He is the Editor-in-Chief of *Computer Networks* (Elsevier) journal, and the founding Editor-in-Chief of the *Ad Hoc Networks* (Elsevier) journal, the *Physical Communication* (Elsevier) journal and the *Nano Communication Networks* (Elsevier) journal. He is an ACM Fellow (1997). He received numerous awards from IEEE and ACM. His current research interests are in nanonetworks, terahertz band communication, software defined networking, 5G cellular systems and wireless underground sensor networks.